nature energy

ARTICLES

https://doi.org/10.1038/s41560-021-00833-6

Free-standing ultrathin lithium metal–graphene oxide host foils with controllable thickness for lithium batteries

Hao Chen[1,6], Yufei Yang[1,6], David T. Boyle[2], You Kyeong Jeong[1], Rong Xu[1], Luize Scalco de Vasconcelos[3], Zhuojun Huang[1], Hansen Wang[1], Hongxia Wang[1], Wenxiao Huang[1], Huiqiao Li[1], Jiangyan Wang[1], Hanke Gu[1], Ryuhei Matsumoto[4], Kazunari Motohashi[4], Yuri Nakayama[4], Kejie Zhao[3] and Yi Cui[1,5]✉

Thin (≤20 μm) and free-standing Li metal foils would enable precise prelithiation of anode materials and high-energy-density Li batteries. Existing Li metal foils are too thick (typically 50 to 750 μm) or too mechanically fragile for these applications. Here, we developed a facile and scalable process for the synthesis of an ultrathin (0.5 to 20 μm), free-standing and mechanically robust Li metal foil within a graphene oxide host. In addition to low areal capacities of ~0.1 to 3.7 mAh cm^{-2}, this Li foil also has a much-improved mechanical strength over conventional pure Li metal foil. Our Li foil can improve the initial Coulombic efficiency of graphite (93%) and silicon (79.4%) anodes to around 100% without generating excessive Li residue, and increases the capacity of Li-ion full cells by 8%. The cycle life of Li metal full cells is prolonged by nine times using this thin Li composite anode.

Lithium-ion batteries, recognized with the Nobel Chemistry Prize in 2019, are critical for consumer electronics, electric vehicles and stationary storage. Further improvements of the energy density of Li-ion batteries are a grand challenge within the field[1–5]. Li metal is considered the ultimate anode for next-generation batteries due to its high theoretical capacity (3,860 mAh g^{-1}) and low reduction potential (−3.04 V versus the standard hydrogen electrode). However, Li metal anodes face two fundamental challenges: first, Li metal is highly reactive, and second, the Li metal anode undergoes extreme volume changes during cycling[3,5]. Several effective solutions, such as host materials[6], artificial solid electrolyte interphase (SEI)[5] and advanced electrolytes[7], have significantly improved the cycle life of metallic Li anodes.

Despite this progress in electrode stabilization, the excessive capacities and thickness of the available Li metal foils remain a critical yet unresolved challenge in this field[4,8]. A practical Li metal battery (LMB) requires a thin Li metal foil with an areal capacity of less than 4 mAh cm^{-2} to pair with common lithium transition metal oxide cathodes (having an areal capacity of 3 to 4 mAh cm^{-2})[4,9]. This requires the thickness of Li metal to be ≤20 μm (Supplementary Note 1). Additionally, conventional Li-ion batteries form a SEI on the anode. The formation of the SEI causes a loss of active Li and capacity (≤1 mAh cm^{-2}) in the first cycle[10], calling for an even thinner Li metal foil (≤5 μm thick) for an ideal Li compensation purpose to achieve 100% initial Coulombic efficiency (ICE) in the conventional anode (defined as precise prelithiation). The recent anodeless LMBs have high energy density but low Coulombic efficiencies in the initial several cycles, leading to fast Li loss and capacity decay in the initial cycles[11]. Adding a thin Li metal foil to the cell could compensate for this Li loss without sacrificing energy density[12–14].

However, existing extrusion-based fabrication technologies[15] are capable of producing Li metal foils with thicknesses of only 20 to several hundreds of micrometres[4,16]. Extruding free-standing Li metal foils that are less than 20 micrometres thick presents the challenge of mechanical fragility and micro-scale manufacture capability. These thick Li foils have severely limited the energy density of LMBs (Supplementary Fig. 1). Electrochemical deposition[17] and vacuum evaporation[18] of Li are the main methods for fabricating micrometre-thin Li, but these methods are costly and rely on heavy substrates, limiting their practicability. A simple and low-cost process for preparing free-standing thin Li metal foils is a critical and unresolved challenge that requires a new technology.

Here, we developed a process that generates an ultrathin, free-standing Li metal foil. First, we use a tunable calendaring process to decrease the thickness of a reduced graphene oxide (rGO) to 0.3 to 20 μm. We then load metallic Li by edge-contacting molten Li to the rGO. As a result, Li is distributed inside the internal channels of the rGO while the rGO retains the micrometre-scale thickness. The thickness of the obtained Li foils ranges from 0.5 to 20 μm (corresponding to ultralow areal capacities of 0.089 to 3.678 mAh cm^{-2}), which breaks the limitations of commercially available Li films (20 to 750 μm thick, 4 to 150 mAh cm^{-2} capacity). Moreover, our Li foils also exhibit increased mechanical strength (525% increase in hardness for resisting permanent plastic deformation), free-standing ability and flexibility. The tunable and ultralow capacity of this Li metal film makes it ideal for compensating for the initial loss of Li in both graphite anodes and silicon anodes. When this film is used, the initial 8% capacity loss is recoverable in conventional Li-ion full cells. In LMBs, the three-dimensional (3D) host structure of the thin foils guides highly reversible Li dissolution/deposition and

[1]Department of Materials Science and Engineering, Stanford University, Stanford, CA, USA. [2]Department of Chemistry, Stanford University, Stanford, CA, USA. [3]School of Mechanical Engineering, Purdue University, West Lafayette, IN, USA. [4]Murata Manufacturing, Nagaokakyo-shi, Japan. [5]Stanford Institute for Materials and Energy Sciences, SLAC National Accelerator Laboratory, Menlo Park, CA, USA. [6]These authors contributed equally: Hao Chen, Yufei Yang. ✉e-mail: yicui@stanford.edu

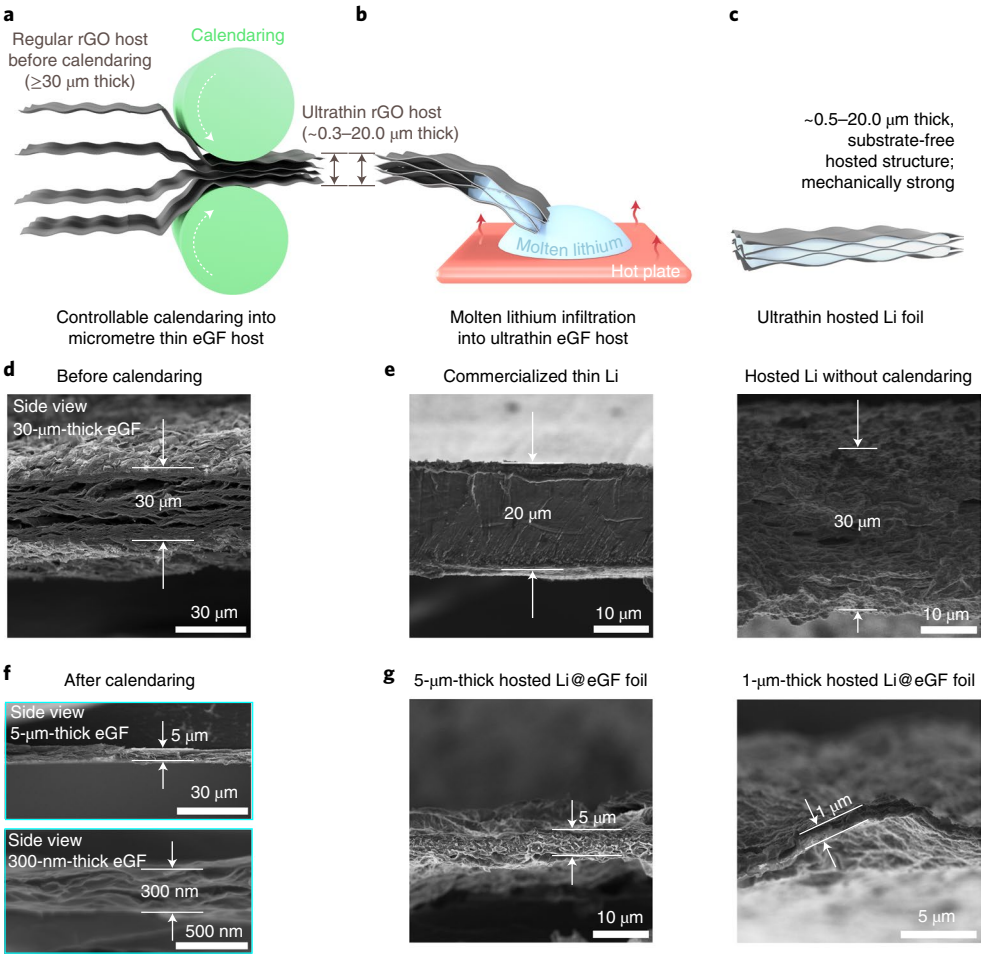

Fig. 1 | Design and fabrication of micrometre-scale thin host and Li metal film. a, Controllable calendaring process for thick and porous eGF films into micrometre-scale thin eGF hosts. **b**, Molten Li infiltration into the ultrathin host to fabricate ultrathin Li@eGF, annealed on a 350 °C hotplate inside a glove box. **c**, Final product of ultrathin, free-standing, strong and thickness-tunable Li@eGF foils. **d**, Cross-sectional SEM image of the common thick host before calendaring. **e**, Cross-sectional SEM images of commercialized 20-μm-thick (that is, thin) Li metal foil (left), and common 30-μm-thick hosted Li@eGF film without preliminary calendaring (right). **f**, Cross-sectional SEM images of submicrometre-scale ultrathin host after controllable calendaring. **g**, Cross-sectional SEM images of fabricated ultrathin 1-μm-thick and 5-μm-thick hosted Li@eGF films after preliminary calendaring process.

prevents rapid fracture of the anode, enabling a cycle life that is prolonged by nine times.

Ultrathin robust free-standing Li composite film fabrication

There are three key steps for the fabrication of ultrathin Li films. First, an ultrafast self-expansion and reduction (USER) reaction[19] of dense graphene oxide (GO) stacks it into a porous, expanded and reduced graphene oxide film (eGF) as the lithium host. Second, a micrometre-scale thickness is made possible by controlled calendaring of the lithium host (Fig. 1a). Third, the composite is fabricated by edge-contacting molten Li absorption into the host (Fig. 1b,c).

The GO film is chosen because it makes the process scalable and it has good mechanical strength and flexibility (Supplementary Fig. 2a,b and Supplementary Video 1). By contacting the edge of the GO film with a 350 °C hotplate inside an inert atmosphere glove box, the USER reaction immediately starts from the touchpoint and rapidly spreads across the whole film within milliseconds (Supplementary Fig. 2c and Supplementary Video 2). This reaction is due to the fast decomposition of abundant oxygen-containing functional groups in GO into carbon monoxide and dioxide gases when superheated (Supplementary Fig. 2d,e). The highly exothermic nature of the USER reaction makes it spread easily across the GO film from a single touchpoint. These internally generated gases were quickly released to create high porosity submicrometre-level channels inside the eGF, thus expanding the film thickness[19]. After the USER reaction, the film expands from a less than 1-μm-thick GO film to a ≥30-μm-thick eGF. Abundant submicrometre-sized channels are also generated inside the eGF as confirmed by both cross-sectional scanning electronic microscope (SEM) images and Brunauer–Emmett–Teller surface area analysis (Supplementary Fig. 3). This 3D porous and lithiophilic eGF is a promising Li host, but the film is too thick (≥30 μm; Fig. 1d and Supplementary Fig. 3) and is not easily controlled during the USER reaction. Direct infusion of Li into a thick host (≥30 μm in eGF, 50 to 800 μm thick in previously reported hosts[6,20–23]) generates a thick Li foil (≥30 μm thick; right in Fig. 1e). As a result, these films have the same problems with energy density as pure Li metal foils of the same thickness.

To solve this thickness issue, we developed a host compression procedure with micrometre-scale precision (Fig. 1a) by using a rolling press (Supplementary Fig. 4a and Supplementary Video 3). The thickness of eGF is tunable from the initial 30 μm to thicknesses of 300 nm and 5 μm (Fig. 1f) by simply controlling the distance between each roller. These thicknesses are one to three orders of magnitude thinner than previously reported hosts (50 to 800 μm thick)[6,20–23]. Despite the compression, submicrometre-wide channels

still exist in the porous eGF after calendaring, which allow for Li infiltration. After compression, contacting the edge of the ultrathin eGF film with molten Li (Fig. 1b) causes rapid capillary absorption of metallic Li into the eGF and turns the material into a Li-metal-containing Li@eGF film (Supplementary Fig. 4b and Supplementary Video 4). This rapid molten Li infusion process is due to the high lithiophilicity (from oxygen-containing functional groups in rGO) and abundant submicrometre channels in eGF, and is not achievable with common hard carbon or carbon nanotube materials (Supplementary Fig. 4c–e). This edge-contact Li absorption approach avoids complete immersion of the material with Li and stores Li only within the channels of the host, rather than on the surface[22,23]. Hence, the Li@eGF film retains its micrometre-scale thickness and free-standing ability.

This fabrication procedure does not require any sacrificial electrolyte or materials, while only the last step of molten Li infusion demands an argon atmosphere. These advantages greatly benefit its cost effectiveness and scalability over common thin Li metal film products, produced by electrochemical deposition, vacuum evaporation and multi-step calendaring methods, and demanding a large volume of costly argon or vacuum-atmosphere-based manufacturing (Supplementary Table 1). Compared with thick commercialized Li metal films (20, 50 and >100 μm thick; Supplementary Fig. 5) and previously reported Li composite electrodes (30 to 800 μm thick; Fig. 1e)[6,20–23], our process reliably makes free-standing Li@eGF films with thicknesses of 1 and 5 μm (Fig. 1g), illustrating a promising micrometre-scale electrode manufacturing strategy for the Li battery industry.

The thickness of Li@eGF electrodes can be further tuned with submicrometre-scale control. Controlling the distance between the rollers during calendaring, the thickness of the porous eGF hosts is tunable to be around 0.3, 1, 2, 5, 10 and 20 μm (Fig. 1d and Supplementary Figs. 6 and 7). Edge-contact infusion of Li into these ultrathin hosts makes flexible and free-standing Li@eGF electrodes with thicknesses of 0.5, 1, 2, 5, 10 and 20 μm, respectively (Fig. 1g and Fig. 2a–e). These procedures and electrodes solve the limitations of controllably preparing thin Li metal foils at micrometre-level thickness. Cross-sectional SEM images (Fig. 2a–e), top-view SEM images (Supplementary Fig. 8), X-ray diffraction spectra and X-ray photoelectron spectroscopy (XPS) spectra (Supplementary Fig. 9) demonstrate that most of the original submicrometre-wide void channels in eGF hosts were filled with metallic Li, supporting the successful fabrication of a micrometre-thin hosted metallic Li composite electrode. These micrometre-level thicknesses of Li@eGF allow for a wide range of areal capacities: 0.089, 0.196, 0.391, 0.853, 1.896 and 3.678 mAh cm^{-2} when charged to 1.5 V (corresponding to 0.5-, 1-, 2-, 5-, 10- and 20-μm-thick Li@eGF films, respectively; Fig. 2f). For comparison, the areal capacities of the thinnest available pure Li metal films (20 and 50 μm thick) are 4 and 10 mAh cm^{-2}, respectively (Supplementary Fig. 5a–c). In addition, 40- to 60-μm-thick free-standing Li@eGF electrodes can also be easily fabricated by increasing the thicknesses of the GO film and eGF host beforehand, affording controllable areal capacities of 8 to 12 mAh cm^{-2}. These higher capacities of Li@eGF anodes would be particularly suitable for high-loading Li–S battery applications (Supplementary Fig. 5d–g). The Li@eGF electrodes have similar electrochemical properties and similar voltage–capacity profiles to pure Li metal, suggesting no compromise to battery operation voltage.

The mechanical strength of the Li@eGF electrode is much stronger than that of pure Li metal films, which is important for the processing of ultrathin electrodes. Representative force–displacement responses of indentations on the electrodes show that the indentation force on Li@eGF was around 150% higher than that on pure Li with the same indentation depth (Fig. 2g), indicating the mechanical strength of the Li@eGF is improved compared with Li. Hosted Li@eGF films also have higher hardness (41.13 MPa) than pure Li (6.58 MPa; Fig. 2h)[24,25], suggesting they are more resistant to plastic deformation induced by shear flow, which is the most common mechanical degradation mechanism of Li metal film. The elastic modulus of Li@eGF (9.34 GPa) is also about 48% higher than pure Li (6.31 GPa; Fig. 2h)[24–26]. Furthermore, the tensile strength (11.41 MPa) and Young's modulus (738.87 MPa) of the Li@eGF film are also much higher than those of pure Li metal film (1.814 MPa in tensile strength and 110.56 Mpa in Young's modulus; Supplementary Fig. 10). In addition to these properties, ultrathin Li@eGF films have excellent flexibility and retain their original shape and function after rolling (Fig. 2i and Supplementary Video 5). Together, these results indicate that the 3D eGF matrix provides superior durability and recoverability of Li, which is important for the practical operation and assembling of thin electrodes. The improved mechanical strength and flexibility of ultrathin Li@eGF electrodes are encouraging for their future application in the battery industry.

Precise prelithiation on graphite anode

Benefiting from their ultralow and tunable capacity, these Li@eGF foils are ideal for prelithiating Li-ion battery anodes (Fig. 3a). Their tunable thickness makes precise compensation of the capacity loss in conventional Li-ion batteries from SEI formation possible[10,27]. Without prelithiation, graphite||Li half cells have a relatively low ICE of around 93%, suggesting ~7% of the available Li is consumed by SEI formation. This loss corresponds to a deviation of ~0.25 mAh cm^{-2} between first cycle charge/discharge capacity, in a graphite anode with mass loading of 8.65 mg cm^{-2}. By covering a 2-μm-thick Li@eGF film (containing a capacity of 0.391 mAh cm^{-2}) on the top surface of a graphite anode, the Li@eGF film partially prelithiates the graphite and compensates this initial Li loss. The ICE of the prelithiated graphite anode improves to 100% (Fig. 3a–c), suggesting that this 2-μm-thick Li@eGF film fully compensates for the initial Li loss amount in graphite anodes. A 5-μm-thick Li@eGF film (0.853 mAh cm^{-2}) raises the ICE to 117.6%, suggesting excessive Li compensation that will lead to metallic Li deposition in the graphite anode. Importantly, precisely prelithiated graphite anodes exhibit no obvious compromise in anode cycling stability (Supplementary Fig. 11) and have excellent consistency between batches (Fig. 3c). These results suggest Li@eGF additives for precise prelithiation could be more practical than current electrochemical prelithiation processes[27–30].

The precise prelithiation with ultrathin Li@eGF films allows for full recovery of the irreversible SEI-based capacity loss in Li-ion full cells (Fig. 3d). The prelithiation improves the capacity of full Li-ion cells with graphite anodes (3.22 mAh cm^{-2}) and a lithium iron phosphate (LFP) cathode (~3.22 mAh cm^{-2}). Without prelithiation, this Li-ion full cell has a theoretical capacity of 3.22 mAh cm^{-2}, but it actually had a lower capacity of 2.97 mAh cm^{-2}. This capacity loss is due to the initial SEI formation on the anode (Supplementary Fig. 1)[10,27], as demonstrated by the consistency between the deviation (0.25 mAh cm^{-2}) and aforementioned initial Li loss amount in graphite anodes. By coating a 2- or 5-μm-thick Li@eGF film on a graphite anode, the capacities of Li-ion full cells are fully recovered and stabilized at the theoretical capacity (around 3.22 mAh cm^{-2}). As a result, the full-cell ICE improves from 87% to around 96% (Fig. 3e and Supplementary Fig. 12), illustrating that this prelithiation function significantly improves the cell capacity and compensates for the initial loss of Li in the anode.

Considering the balanced negative:positive (N:P) capacity ratio requirement in full-cell configurations, the capacity of the prelithiation additive must be precisely controlled to avoid excessive Li deposition on the anode, which prevents poor battery performance and safety hazards[31]. Prelithiation with 5-μm-thick Li@eGF (0.853 mAh cm^{-2}) exceeds the initial Li loss amount of the graphite anode (0.25 mAh cm^{-2}). Expectedly, the full cell suffered from metallic Li plating, because the graphite cannot accommodate all

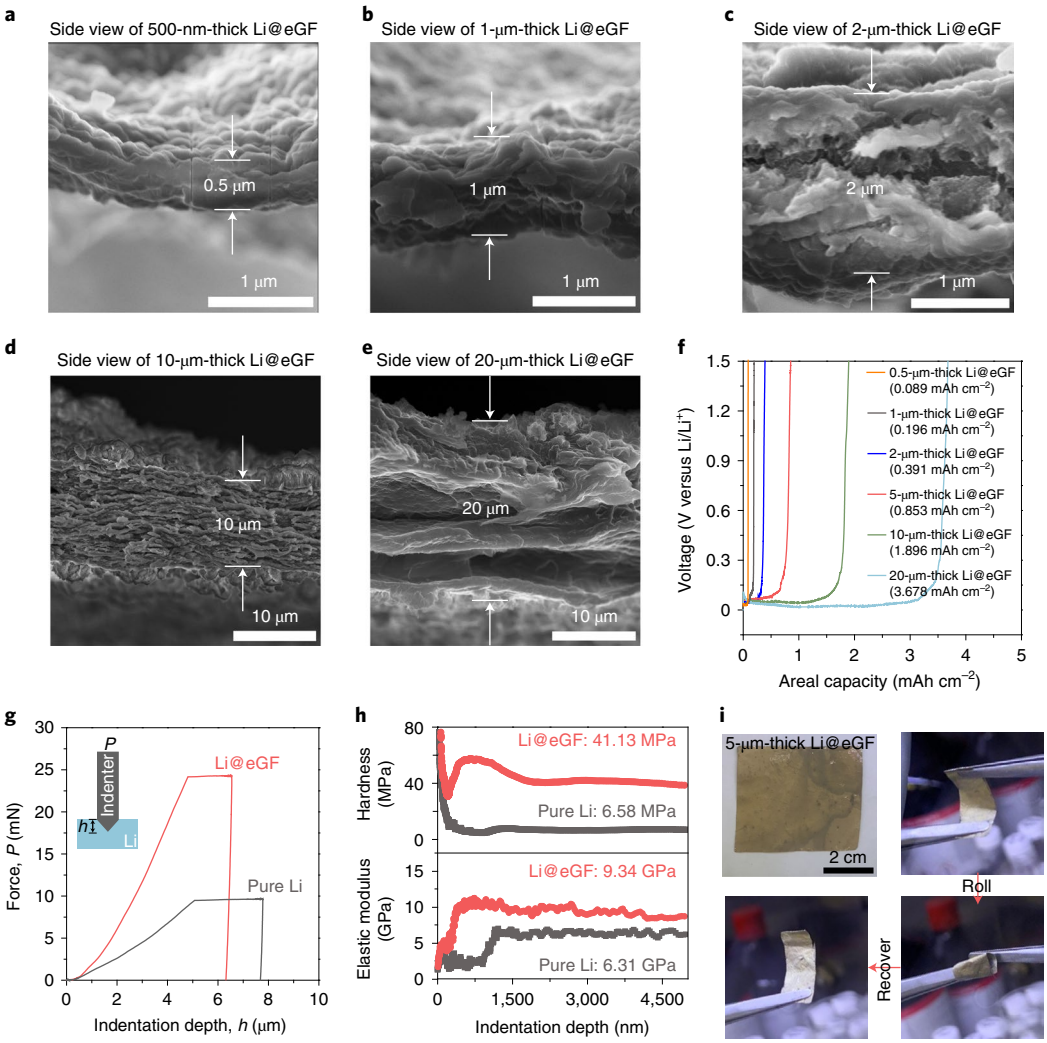

Fig. 2 | Characterizations of the ultrathin Li@eGF film. a–e, Cross-sectional SEM images of ultrathin Li@eGF films, exhibiting tunable thickness from 500 nm to 20 μm. **f**, Full Li stripping curves of ultrathin Li@eGF films charged to 1.5 V versus Li/Li$^+$, showing tunable and low areal capacities with different thicknesses. **g**, Comparisons of mechanical strength between pure Li metal and Li@eGF films using nanoindentation measurements. The inset schematic shows the working mechanism of nanoindentation measurements on Li metal film. **h**, Comparisons of hardness and elastic modulus between pure Li metal and Li@eGF films using nanoindentation measurements. The results obtained in the shallow indentation (<1,500 nm) are oscillating due to the errors induced by the rough surface, while the results obtained in the deep indentation (>1,500 nm) are consistent, indicating a homogeneous distribution of mechanical properties along the thickness direction. **i**, Digital camera photo of centimetre-scale fabricated ultrathin Li@eGF foil (5-μm-thick) and abuse test.

Li ions from the cathode during cell charging. This plating induces higher-voltage plateaus (discharge at ~3.4 V and charge at ~3.5 V; Fig. 3f) because of the metallic Li deposition on the anode (proved by X-ray diffraction spectra; Fig. 3g). By contrast, the graphite || LFP full cell prelithiated with 2-μm-thick Li@eGF shows no evidence of metallic Li plating, demonstrating that all Li ions were accommodated by the graphite anodes. Top-view SEM images further show that Li dendrites were plated on the anode when the 5-μm-thick Li@eGF is used (Fig. 3h), whereas graphite prelithiated with 2-μm-thick Li@eGF has a clean surface without any Li dendrites (Fig. 3i). These results demonstrate the importance of precisely tuning the micrometre-level thickness of Li metal electrodes for prelithiation.

Precise prelithiating and stabilizing nano-silicon anode

The tunable thickness of micrometre-thin Li@eGF makes it ideal for prelithiating advanced nano-silicon anodes. Si has a high theoretical capacity (4,200 mAh g^{-1}), but it also has a low ICE (~79.4% in the Si nanoparticle anode). This low ICE corresponds to a deviation of ~0.8 mAh cm^{-2} between capacities of the first cycle charge/discharge in a nano-Si anode with mass loading of 1.2 mg cm^{-2} (Fig. 4a and Supplementary Fig. 11c)[32,33]. The 5-μm-thick Li@eGF is the most desired thickness for prelithiating this nano-Si anode, as its capacity (0.853 mAh cm^{-2}) precisely matches the initial Li loss amount to improve the anode ICE to 100.5% (Fig. 4b). The 2-μm-thick Li@eGF (0.391 mAh cm^{-2}) only partially compensates the Li loss and results in an ICE of 88.1%. Prelithiated Si anodes have similar voltage profiles to Si anodes without prelithiation, demonstrating that there is no compromise to electrochemical behaviour or kinetics of the anode (Fig. 4c). The successful prelithiation of both conventional graphite and advanced nano-Si anodes by Li@eGF proves its universality as a prelithiation material for Li-ion batteries.

In addition to the prelithiation function, the Li@eGF film also minimizes the volume-expansion-induced cracking[33] and improves the cycling stability of nano-Si anodes. Covering the top surfaces of the anodes with the 2- and 5-μm-thick Li@eGF improves their specific capacities to 2,406 and 2,565 mAh g^{-1}, respectively (Fig. 4d),

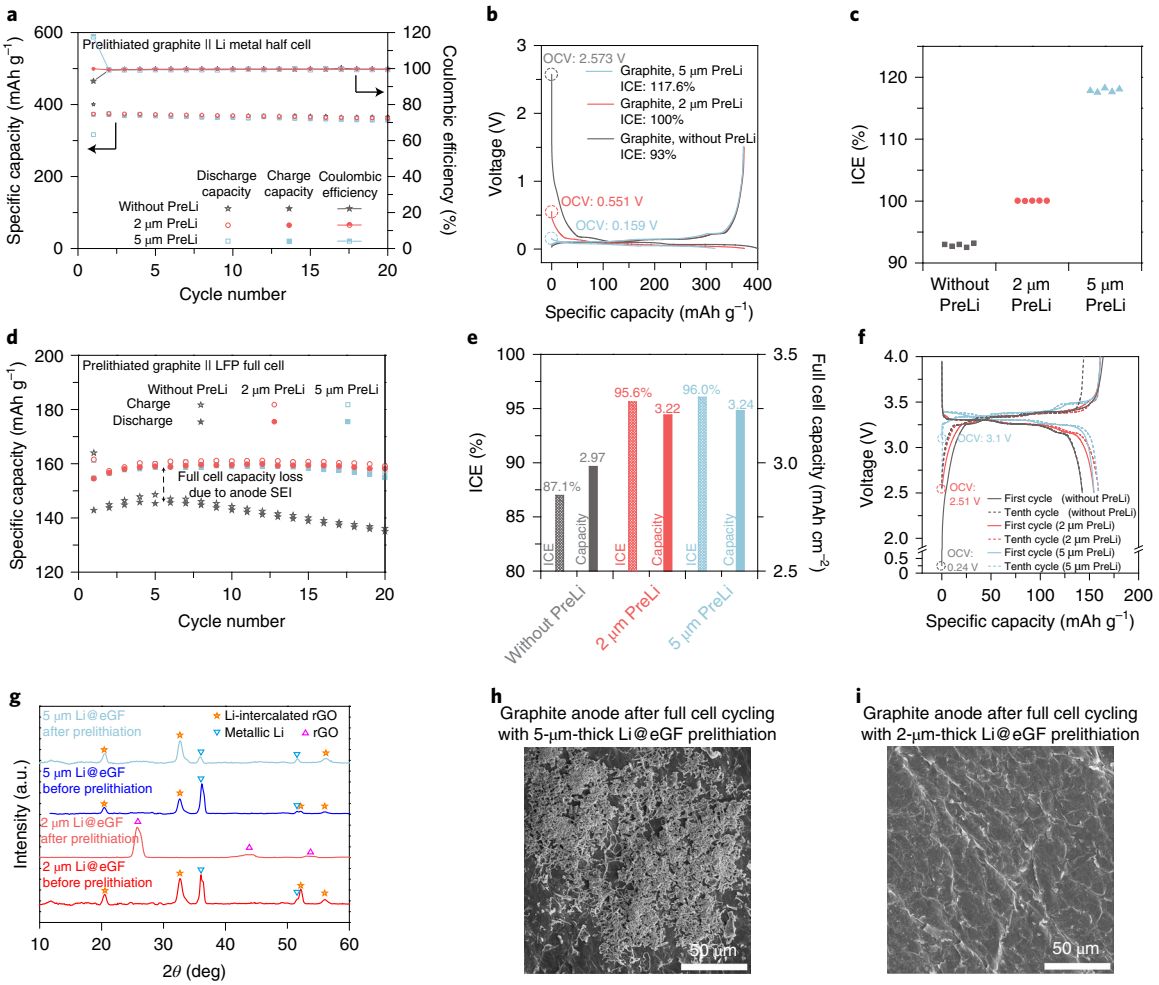

Fig. 3 | Ultrathin Li@eGF film enables precise prelithiation and ideal ICE of graphite anode. a, Galvanostatic cycling of graphite electrodes at 0.05 C using different thicknesses of Li@eGF films for prelithiation (PreLi). Solid lines represent Coulombic efficiencies, and dots represent capacities. For this graphite||Li metal half cell, 1C = 372 mA g^{-1}. **b**, Voltage profiles of graphite electrodes in the first cycle, using different thicknesses of Li@eGF film for prelithiation. The decreased open circuit voltages (OCVs) (indicated by dashed circles) were due to the reduced electrochemical potentials of lithiated graphite. **c**, Summary of the ICE numbers of multiple graphite electrodes using different thicknesses of Li@eGF film for prelithiation; five parallel samples were recorded for each prelithiation condition. **d**, Galvanostatic cycling of graphite || LFP full cells at 0.05 C using different thicknesses of Li@eGF film for prelithiation in the anode. For this graphite||LFP full cell, 1C = 150 mA g^{-1}. **e**, Comparisons of the ICE and areal capacity (after five activation cycles) of graphite || LFP full cells using different thicknesses of Li@eGF film for anode prelithiation. **f**, Voltage profiles of graphite || LFP full cells at 0.05 C using different thicknesses of Li@eGF film for prelithiation. **g**, X-ray diffraction spectra of the Li@eGF film before prelithiation and after prelithiation cycle (at full-cell charged state). θ, the incidence angle. **h**,**i**, Top-view SEM images of the Li@eGF-coated anode from graphite || LFP full cells after cycling at a charged state.

with 80% capacity retention after ten cycles (Fig. 4a) and 56% retention after 100 cycles (Supplementary Fig. 13). These metrics far surpass the performance of the nano-Si anode without Li@eGF coatings (specific capacity of 2,225 mAh g^{-1} with 57% retention after ten cycles). SEM images further show obvious cracks at both the submillimetre and submicrometre scales in the uncoated nano-Si electrode after ten cycles (right side in Fig. 4e, Fig. 4f and Supplementary Fig. 13c,d). These cracks suggest that the large volume change of Si nanoparticles during cycling causes the disconnection of the active materials and large losses of capacity (Fig. 4h)[32]. By comparison, the Si nanoparticles beneath the Li@eGF coating had excellent integrity after cycling (left side in Fig. 4e,g and Supplementary Fig. 13e,f). This absence of cracking is due to a unique double-protection function of the Li@eGF film after prelithiation, which maintained the original 3D continuous and porous structure of eGF after all of the metallic Li component was extracted away for prelithiation (Fig. 4i and Supplementary Fig. 13g): the conductive eGF film acts as a secondary current collector for active material utilization, and the continuous and robust eGF film tightly holds the surficial Si nanoparticles together to resist the disconnection of active materials. Therefore, our Li@eGF can provide not only tunable prelithiation capabilities, but also a double-protection function for the utilization and stabilization of high-volume-change electrode materials.

Thin yet stable Li composite anode for Li metal full cell

The advantages of the 3D lithiophilic host, micrometre-level thickness and improved mechanical strength make this Li@eGF film a strong candidate as a thin and stable Li metal anode for practical high-energy-density LMBs[4,34]. In a single-layer pouch cell using a commercially available 20-μm-thick pure Li metal anode (~4 mAh cm^{-2}) and a LFP cathode (3.24 mAh cm^{-2}), fast battery failure was always observed at early cycles (Fig. 5a). This failure starts as a sudden voltage drop during the discharging step in the 21st

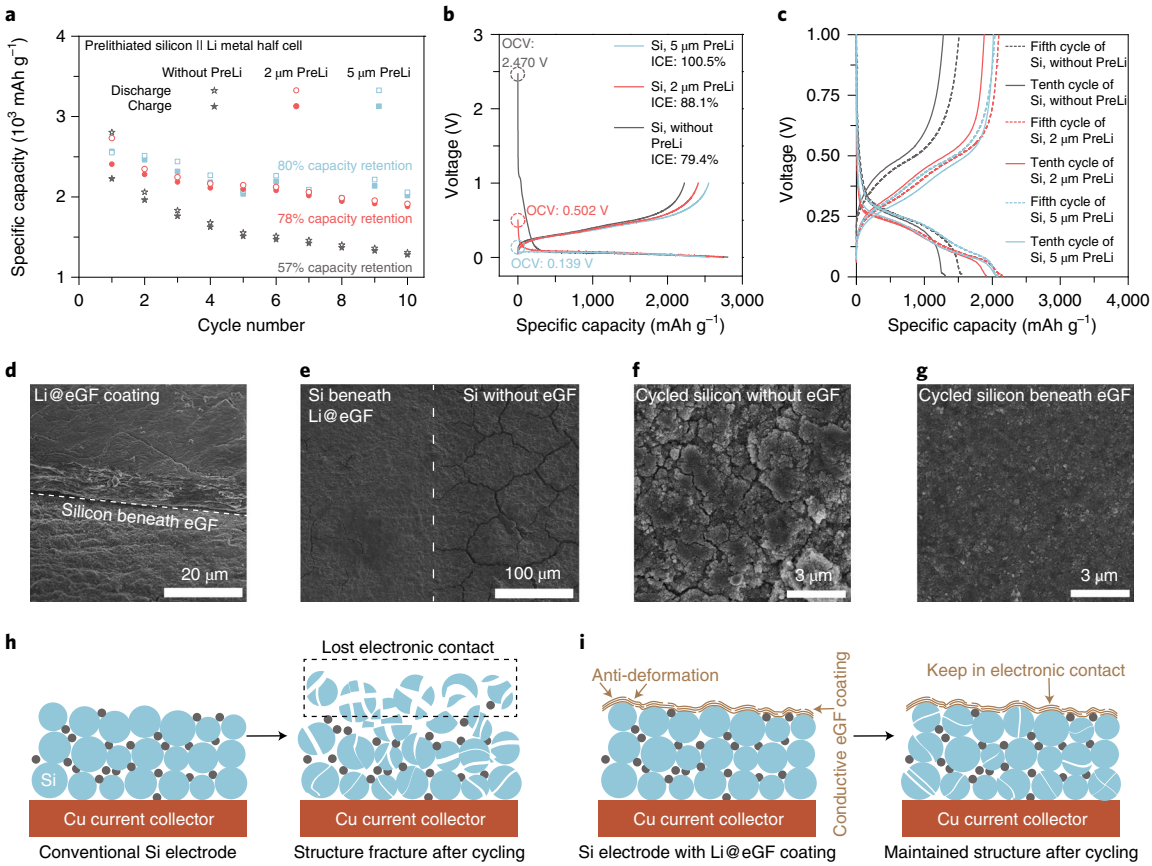

Fig. 4 | Ultrathin Li@eGF film improved initial ICE and cycling stability of Si anode. a, Galvanostatic cycling of Si electrodes at 0.05 C using different thicknesses of Li@eGF films for prelithiation. **b**,**c**, Voltage profiles of Si electrodes using different thicknesses of Li@eGF film in the first cycle (**b**) and in the fifth and tenth cycle (**c**). The decreased OCVs (dashed circles) indicate an increased level of prelithiation with a larger amount of lithium hosted in Li@eGF. **d**, A 45° sloped SEM image of the Si anode, protected by 5-μm-thick Li@eGF. The Li@eGF covering the Si was half removed, and this image shows the boundary between the covered and removed parts. **e**, Top-view SEM image of cycled Si anode with left side covered by protective Li@eGF film. The covered Li@eGF was removed before SEM characterization to inspect the Si particles underneath the Li@eGF. **f**,**g**, Comparison between morphologies of cycled Si anode without protection (**f**) and covered by protective Li@eGF film (**g**). The covered Li@eGF was removed before SEM characterization to inspect the Si nanoparticles underneath the Li@eGF. **h**, Electrode failure mechanism of conventional nano-Si anode without protection layer. **i**, Protection mechanism of Li@eGF film for Si anode.

cycle (Fig. 5b), and the battery circuit broke with full capacity loss in subsequent cycles (that is, they have no charge/discharge capacity at all; Supplementary Fig. 14). This battery circuit-break failure during discharging is totally different from the commonly accepted failure mechanisms of LMBs[3–5] (that is, dendrite-induced short-circuit during cell charging[35] and gradual Li depletion after long cycling[36]; Supplementary Fig. 15).

To explain this failure mode, the 20-μm-thick pure Li metal anode was extracted from the pouch cell after 20 cycles. Holes and cracks that disconnected from the anode are apparent across much of the electrode (Fig. 5d). SEM images illustrate that these cracks gradually merge in the initial cycles and broaden during subsequent cycles (Fig. 5e, Supplementary Fig. 16), suggesting that they are caused by the uneven electrochemical stripping of metallic Li during repeated discharging steps[37]. These growing cracks rapidly separate the original thin Li metal anode into several parts of 'dead Li'[16] and disconnect large pieces of the active Li metal electrode material from the final tab current collector, long before depletion of active materials[4].

Replacing the pure Li metal film with a 20-μm-thick Li@eGF film greatly improves the cycling stability (Supplementary Fig. 17). The fabricated Li@eGF||LFP full cell retains 81% of its capacity after 200 cycles (Fig. 5a), with only a tiny increase in overpotential (Fig. 5c). Importantly, digital photos and SEM images show the absence of cracks and retention of the original 3D continuous structure in this 20-μm-thick Li@eGF anode after 200 cycles (Fig. 5f,g and Supplementary Fig. 17). The improved stability of the Li@eGF electrode is attributed to its unique characteristics: (1) the uniform distribution of metallic Li in the 3D lithiophilic rGO matrix suppresses the inhomogeneity of local current density, restricts the uneven stripping of Li and improves the Li plating/stripping reversibility (Supplementary Fig. 18a), which is uncontrollable and self-aggravated in pure Li metal anodes[6]; (2) the low weight ratio and high conductivity of the rGO matrix provides a current-collecting function, even when Li metal species are all stripped away; and (3) the high mechanical strength of the Li@eGF also suppresses the inhomogeneous electrochemical plating and stripping during cycling[38]. Therefore, this ultrathin hosted Li@eGF film improves both the cycling stability of thin Li-metal-anode-based full cells and the energy density of the cell, and these improvements are achievable in both carbonate and ether electrolyte systems (Supplementary Fig. 18).

Conclusions

In summary, we have developed a process to fabricate micrometre-thin, free-standing and hosted Li metal films and demonstrate their applications for prelithiation and high-energy-density LMBs. Infusing

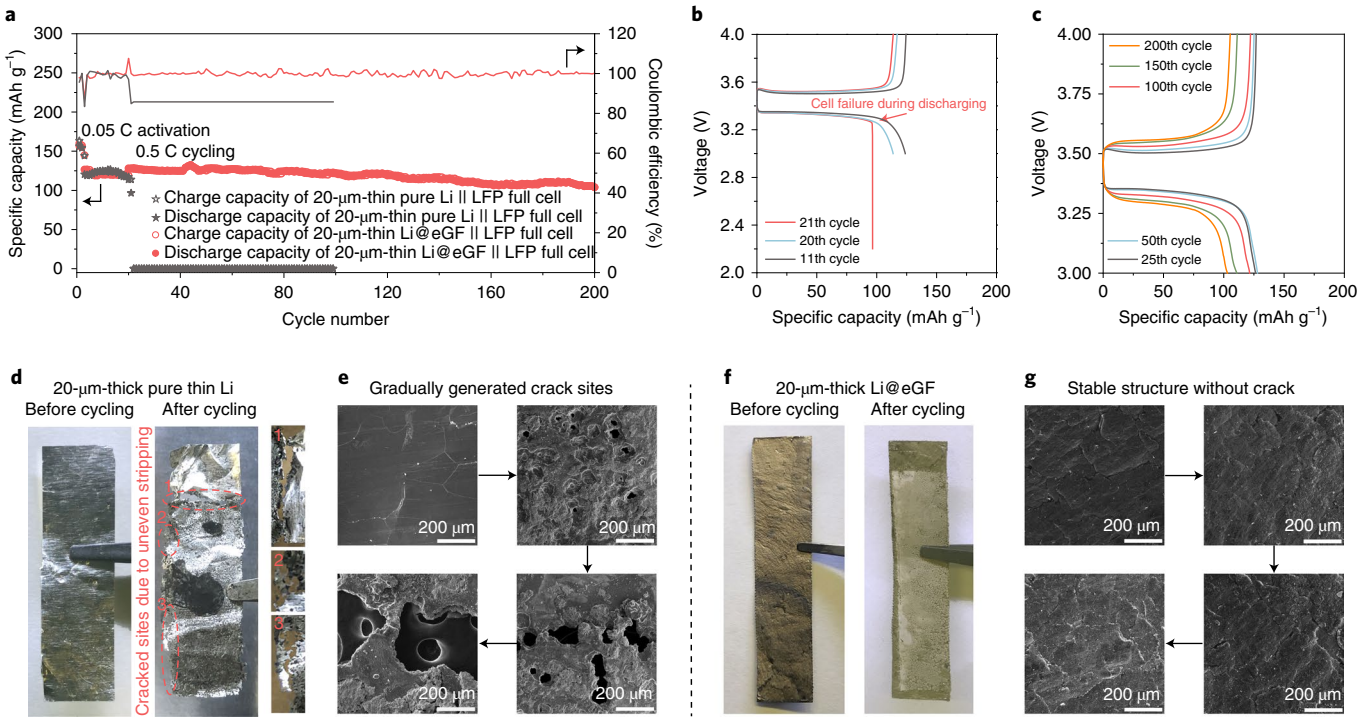

Fig. 5 | Ultrathin Li@eGF film improves stability of Li metal || LFP full cell. a, Galvanostatic cycling of LFP pouch cell with ultrathin Li foil and Li@eGF film with initial two activation cycles at 0.05 C and long cycling at 0.5 C. 1C = 150 mA g^{-1}. **b**,**c**, Voltage profiles of LFP full cells after different cycles, using 20-μm-thick pure Li metal foil (**b**) or 20-μm-thick Li@eGF film (**c**). **d**, Digital camera photos of 20-μm-thick pure Li foil before and after 20 cycles in pouch cell, showing that non-uniform cracks and fissures were gradually broadened to rupture the original film. **e**, Top-view SEM images of 20-μm-thick pure Li foil before cycling, and after 5, 10 and 20 cycles, as indicated by arrows. The holes and cracks were gradually broadened during these cycles, with a diameter increase from 30 μm to >500 μm. **f**, Digital camera photos of 20-μm-thick Li@eGF film before and after cycling in pouch cell, showing absence of crack. **g**, Top-view SEM images of 20-μm-thick Li@eGF film before cycling, and after 50, 100 and 200 cycles, as indicated by arrows.

molten metallic Li into a host with tunable submicrometre-scale thickness results in an ultrathin Li@eGF film with controllable and ultralow thickness (0.5 to 20 μm) and areal capacity (0.089 to 3.678 mAh cm^{-2}). These thicknesses and capacities are one to three orders of magnitude smaller than those of existing Li metal films. The thinness, ultralow capacity and hosted structure provide many technological possibilities that cannot be satisfied by the existing thick Li metal electrodes. Benefiting from its controllable and ultralow thickness, prelithiation with this Li@eGF film appropriately compensates for the loss of capacity in the initial cycle of graphite (ICE of 93%) and Si anodes (ICE of 79.4%). As a result, these anodes achieve an ideal ICE of ~100% in the first cycle, along with 8% enhanced capacity in Li-ion full cells. The 3D matrix host structure also prevents the rapid rupture of ultrathin Li metal anodes during cycling and improves the cycle life of LMBs by nine times. By reducing the electrode thickness to the micrometre scale and improving anode stability simultaneously, our tunable micrometre-thin and free-standing Li@eGF film provides a pathway for future high-energy-density Li batteries. It also suggests that this micrometre-scale technology could break the limitations of electrode thickness in current manufacturing.

Methods

Preparation of the ultrathin eGF host. Commercially available GO solution (Hangzhou Gaoxi Technology, 9 mg ml^{-1}) was blade-coated onto a glass substrate using a doctor blade, dried at room temperature, peeled off from the glass substrate and transferred into a nitrogen-filled glove box. The USER reaction was conducted by touching the GO film to the 350 °C hotplate inside the glove box (Supplementary Video 2), resulting in rapid reduction and self-expansion. The expanded porous eGF was sandwiched between two stainless-steel or polypropylene films, and calendared into the desired thickness by controlling the distance of the gap between two rollers.

Fabrication of ultrathin Li@eGF electrode. Solid lithium was annealed to 350 °C on a hotplate to prepare a molten lithium droplet inside an argon-filled glove box. The ultrathin lithium-containing Li@eGF anode was prepared by contacting the edge of ultrathin calendared eGF with the molten lithium droplet to absorb lithium into the host, as shown by Supplementary Video 4.

Electrochemistry. The performances of half cells with prelithiated anodes were evaluated with the galvanostatic cycling of cells (CR-2032). Graphite or Si anodes (1 cm^2) were used as working electrodes assembled in an argon-filled glove box, with pure lithium metal foil (1 cm^2) as counter electrodes. The performances of full cells with prelithiated anodes were evaluated by the galvanostatic cycling of coin cells with the graphite anode and LFP cathode (1 cm^2). The ultrathin Li@eGF (1 cm^2) was placed on top of a graphite or Si working anode for prelithiation. One layer of Celgard separators (Celgard 2325, 25 μm thick) was used to separate the electrodes. The carbonate electrolyte was prepared by dissolving 1 M $LiPF_6$ in 1:1 (v/v) ethylene carbonate (BASF) and diethyl carbonate (BASF) with 1% vinylene carbonate and 10% fluoroethylene carbonate as additives. The 50 μl electrolyte was added onto the cathode and separator during cell assembly. Battery cycling data were collected using LAND and Arbin eight-channel battery testers at room temperature.

Lithium metal || LFP pouch cells were fabricated inside an argon-filled glove box, using 20-μm-thin Li foil or Li@eGF film as the anode, an LFP cathode and one layer of Celgard 2325 separator. The LFP cathode was connected to an aluminium tab by welding, while the lithium foil was connected to a nickel tab by adhering and pressing inside the argon-filled glove box. A controlled amount of carbonate electrolyte (10 g Ah^{-1}) was injected into the pouch cells inside the argon-filled glove box, followed by vacuum sealing. The fabricated batteries were rested for 24 h before cycling. Battery cycling data were collected using a VMP3 potentiostat (Biologic) at room temperature.

Graphite anodes were prepared by mixing graphite powder (MTI) with polyvinylidene fluoride (MTI) and carbon black (TIMCAL) at a weight ratio of 92:2:6 using *N*-methyl-2-pyrrolidone (NMP) solvent. The slurry was blade-coated on copper foil (MTI), dried in an 80 °C vacuum oven and calendared before use. The areal mass loading of graphite was ~8.65 mg cm^{-2}. Si anodes were prepared by mixing nano-Si powder (50 to 100 nm in diameter, MTI) with carboxymethyl cellulose, styrene–butadiene rubber (MTI) and carbon black (TIMCAL) at a

weight ratio of 60:10:10:20 using water as a solvent. The slurry was blade-coated on copper foil (MTI), dried in an 80 °C vacuum oven and calendared before use. The areal mass loading of Si was ~1.2 mg cm^{-2}. LFP cathodes were prepared by mixing LFP powder (MTI) with polyvinylidene fluoride and carbon black (TIMCAL) at a weight ratio of 90:5:5 with NMP solvent. The cathode slurry was blade-coated on conductive carbon-coated aluminium foil (MTI), dried in an 80 °C vacuum oven and calendared before use. The areal mass loading of LFP was ~20.3 mg cm^{-2}.

Characterization. SEM images were taken with an FEI Magellan 400 XHR scanning electron microscope at an acceleration voltage of 5 kV. Focused ion beam SEM images were taken through cross-sectioning a sample with a Ga^+ ion beam and observing with the electron beam on an FEI Helios NanoLab 600i DualBeam focused-ion-beam/SEM. Before SEM characterization, the cycled batteries were disassembled in an argon-filled glove box, then the electrodes were gently rinsed with diethyl carbonate to remove residual salt. X-ray diffraction patterns were recorded on a PANalytical X'Pert instrument with preliminary sample sealing inside an argon-filled glove box. XPS analysis was obtained on a PHI VersaProbe 1 scanning XPS microprobe with an air-free transfer vessel. The binding energies were calibrated with respect to the C 1*s* peak at 284.6 eV. During the USER reaction, the generated gas was collected by a sealed tube covering the GO film, and then injected into a gas chromatograph (SRI 8610C). A Netzsch STA 449 instrument was used for thermogravimetric analysis at a heating rate of 5 °C min^{-1}. Mechanical properties of the samples were measured by a nanoindentation instrument (G200, Keysight) in an argon-filled glove box. A continuous stiffness measurement using a Berkovich indenter was conducted. The elastic modulus and hardness were continuously measured based on the dynamic material stiffness during the indentation loading. The maximum indentation depth on the samples was set to 5 µm. The loading, holding and unloading times were 10, 5 and 10 s, respectively. The hardness and elastic modulus were simultaneously measured using the continuous stiffness measurement during the indentation loading, by which the influence of Li creep could be eliminated. The tensile strength measurement was conducted using an Instron 5565 tester with a 100 N load cell. The width, length and thickness of the sample was 7 mm, 10 mm and 50 µm, respectively. The loading rate was 10 mm min^{-1}.

Data availability

All relevant data are included in the paper and its Supplementary Information. Source data are provided with this paper.

Received: 6 January 2021; Accepted: 19 April 2021;
Published online: 20 May 2021

References

1. Armand, M. & Tarascon, J. M. Building better batteries. *Nature* **451**, 652–657 (2008).
2. Chu, S. & Majumdar, A. Opportunities and challenges for a sustainable energy future. *Nature* **488**, 294–303 (2012).
3. Lin, D., Liu, Y. & Cui, Y. Reviving the lithium metal anode for high-energy batteries. *Nat. Nanotechnol.* **12**, 194–206 (2017).
4. Liu, J. et al. Pathways for practical high-energy long-cycling lithium metal batteries. *Nat. Energy* **4**, 180–186 (2019).
5. Cheng, X.-B., Zhang, R., Zhao, C.-Z. & Zhang, Q. Toward safe lithium metal anode in rechargeable batteries: a review. *Chem. Rev.* **117**, 10403–10473 (2017).
6. Lin, D. et al. Layered reduced graphene oxide with nanoscale interlayer gaps as a stable host for lithium metal anodes. *Nat. Nanotechnol.* **11**, 626–632 (2016).
7. Tikekar, M. D., Choudhury, S., Tu, Z. & Archer, L. A. Design principles for electrolytes and interfaces for stable lithium-metal batteries. *Nat. Energy* **1**, 16114 (2016).
8. Albertus, P., Babinec, S., Litzelman, S. & Newman, A. Status and challenges in enabling the lithium metal electrode for high-energy and low-cost rechargeable batteries. *Nat. Energy* **3**, 16–21 (2018).
9. Chen, S. et al. Critical parameters for evaluating coin cells and pouch cells of rechargeable Li-metal batteries. *Joule* **3**, 1094–1105 (2019).
10. Sun, Y. et al. High-capacity battery cathode prelithiation to offset initial lithium loss. *Nat. Energy* **1**, 15008 (2016).
11. Cheng, Q. et al. Graphene-like-graphite as fast-chargeable and high-capacity anode materials for lithium ion batteries. *Sci. Rep.* **7**, 14782 (2017).
12. Weber, R. et al. Long cycle life and dendrite-free lithium morphology in anode-free lithium pouch cells enabled by a dual-salt liquid electrolyte. *Nat. Energy* **4**, 683–689 (2019).
13. Xiao, J. et al. Understanding and applying coulombic efficiency in lithium metal batteries. *Nat. Energy* **5**, 561–568 (2020).
14. Yu, Z. et al. Molecular design for electrolyte solvents enabling energy-dense and long-cycling lithium metal batteries. *Nat. Energy* **5**, 526–533 (2020).
15. Schmuch, R., Wagner, R., Hörpel, G., Placke, T. & Winter, M. Performance and cost of materials for lithium-based rechargeable automotive batteries. *Nat. Energy* **3**, 267–278 (2018).
16. Shi, P. et al. Electrochemical diagram of an ultrathin lithium metal anode in pouch cells. *Adv. Mater.* **31**, 1902785 (2019).
17. Mashtalir, O., Nguyen, M., Bodoin, E., Swonger, L. & O'Brien, S. P. High-purity lithium metal films from aqueous mineral solutions. *ACS Omega* **3**, 181–187 (2018).
18. Kato, A., Hayashi, A. & Tatsumisago, M. Enhancing utilization of lithium metal electrodes in all-solid-state batteries by interface modification with gold thin films. *J. Power Sources* **309**, 27–32 (2016).
19. Chen, H. et al. Electrode design with integration of high tortuosity and sulfur-philicity for high-performance lithium-sulfur battery. *Matter* **2**, 1605–1620 (2020).
20. Liu, Y. et al. Lithium-coated polymeric matrix as a minimum volume-change and dendrite-free lithium metal anode. *Nat. Commun.* **7**, 10992 (2016).
21. Liang, Z. et al. Composite lithium metal anode by melt infusion of lithium into a 3D conducting scaffold with lithiophilic coating. *Proc. Natl Acad. Sci. USA* **113**, 2862–2867 (2016).
22. Chi, S.-S., Liu, Y., Song, W.-L., Fan, L.-Z. & Zhang, Q. Prestoring lithium into stable 3D nickel foam host as dendrite-free lithium metal anode. *Adv. Funct. Mater.* **27**, 1700348 (2017).
23. Huang, G. et al. Lithiophilic 3D nanoporous nitrogen-doped graphene for dendrite-free and ultrahigh-rate lithium-metal anodes. *Adv. Mater.* **31**, 1805334 (2019).
24. Wang, Y. & Cheng, Y.-T. A nanoindentation study of the viscoplastic behavior of pure lithium. *Scr. Mater.* **130**, 191–195 (2017).
25. Tariq, S. et al. Li material testing - Fermilab Antiproton Source lithium collection lens. In *Proceedings of the 2003 Particle Accelerator Conference* 1452–1454 (IEEE Xplore, 2003).
26. de Vasconcelos, L. S., Xu, R. & Zhao, K. Operando nanoindentation: a new platform to measure the mechanical properties of electrodes during electrochemical reactions. *J. Electrochem. Soc.* **164**, A3840–A3847 (2017).
27. Holtstiege, F., Bärmann, P., Nölle, R., Winter, M. & Placke, T. Pre-lithiation strategies for rechargeable energy storage technologies: concepts, promises and challenges. *Batteries* **4**, 4 (2018).
28. Ren, J. J. et al. Pre-lithiated graphene nanosheets as negative electrode materials for Li-ion capacitors with high power and energy density. *J. Power Sources* **264**, 108–113 (2014).
29. Jang, J. et al. Chemically prelithiated graphene for anodes of Li-ion batteries. *Energy Fuels* **34**, 13048–13055 (2020).
30. Yao, C. et al. An efficient prelithiation of graphene oxide nanoribbons wrapping silicon nanoparticles for stable Li^+ storage. *Carbon* **168**, 392–403 (2020).
31. Tomaszewska, A. et al. Lithium-ion battery fast charging: a review. *eTransportation* **1**, 100011 (2019).
32. Wu, H. & Cui, Y. Designing nanostructured Si anodes for high energy lithium ion batteries. *Nano Today* **7**, 414–429 (2012).
33. Sun, Y., Liu, N. & Cui, Y. Promises and challenges of nanomaterials for lithium-based rechargeable batteries. *Nat. Energy* **1**, 16071 (2016).
34. Niu, C. et al. High-energy lithium metal pouch cells with limited anode swelling and long stable cycles. *Nat. Energy* **4**, 551–559 (2019).
35. Zhang, Y.-j et al. Integrated reduced graphene oxide multilayer/Li composite anode for rechargeable lithium metal batteries. *RSC Adv.* **6**, 11657–11664 (2016).
36. Moorthy, B. et al. Ice-templated free-standing reduced graphene oxide for dendrite-free lithium metal batteries. *ACS Appl. Energy Mater.* **3**, 11053–11060 (2020).
37. Shi, F. et al. Lithium metal stripping beneath the solid electrolyte interphase. *Proc. Natl Acad. Sci. USA* **115**, 8529–8534 (2018).
38. LePage, W. S. et al. Lithium mechanics: roles of strain rate and temperature and implications for lithium metal batteries. *J. Electrochem. Soc.* **166**, A89–A97 (2019).

Acknowledgements

Part of this work was performed at the Stanford Nano Shared Facilities and Stanford Nanofabrication Facility, supported by the National Science Foundation under award ECCS-2026822. Fabrication of the ultrathin Li metal foils and the Li-metal-anode-based full cell applications are funded by Murata Manufacturing. Utilizing the ultrathin Li metal foils to prelithiate the graphite and silicon anode was supported by the Assistant Secretary for Energy Efficiency and Renewable Energy, Office of Vehicle Technologies of the US Department of Energy under the Battery Materials Research programme. Y.C. acknowledges the 20-µm-thick pure Li metal foils provided from Hydro-Québec company.

Author contributions

Y.C. conceived the idea for the project. H.C., Y.Y., Hansen Wang and H.G. designed the experiments and fabricated the electrodes. H.C. conducted the SEM and XPS

characterizations. Hongxia Wang conducted the X-ray diffraction characterization and gas chromatograph measurements. Y.K.J. fabricated the nano-Si electrodes. R.X. and L.S.V. conducted the nanoindentation characterizations. Z.H. and Y.Y. conducted the tensile strength characterizations. Y.Y. and J.W. designed the prelithiation process. H.C. and W.H. fabricated the pouch cells. W.H. collected the video for the USER reaction. H.C. and Y.Y. designed and conducted the electrochemical measurements. H.C., Y.Y., D.T.B., R.X., R.M., K.M., Y.N. and Y.C. wrote and revised the manuscript. All authors discussed the results and commented on the manuscript at all stages.

Competing interests

The authors declare no competing interests.

Additional information

Supplementary information The online version contains supplementary material available at https://doi.org/10.1038/s41560-021-00833-6.

Correspondence and requests for materials should be addressed to Y.C.

Peer review information *Nature Energy* thanks Boštjan Genorio, Tianyou Zhai and the other, anonymous, reviewer(s) for their contribution to the peer review of this work.

Reprints and permissions information is available at www.nature.com/reprints.

Publisher's note Springer Nature remains neutral with regard to jurisdictional claims in published maps and institutional affiliations.